Draft version February 2, 2008
Preprint typeset using LaTeX style emulateapj v. 10/09/06

arXiv:0711.4384v2 [astro-ph] 6 Dec 2007

CREATION OF THE X-RAY CAVITY JET AND ITS RADIO LOBE IN M87/VIRGO WITH COSMIC RAYS; RELEVANCE TO RELIC RADIO SOURCES

William G. Mathews[1] and Fabrizio Brighenti[1,2]

Draft version February 2, 2008

ABSTRACT

Young cavities in the X-ray emitting hot gas in galaxy clusters are often filled with radio synchrotron emission from cosmic rays. However, in the M87/Virgo cluster, where cavities are less prominent, X-ray observations show a 30-kpc long nearly radial filament of relatively cooler gas that projects from the cluster core into a large (40 kpc) radio lobe. We describe the dynamical relationship between these two very dissimilar observations with gas dynamical calculations that include the dynamical effects and spatial diffusion of cosmic rays. After cosmic rays inflate the cavity, they diffuse through the cavity walls, forming a much larger lobe. The cavities, which are most visible just after they have formed (in about 20 Myr), require a total cosmic ray energy that is more than 10 times larger than that usually assumed, $E = 4PV$. During the relatively brief cavity lifetime, a jet-like, low-entropy thermal filament is formed in the buoyant flow and moves at high subsonic velocities through the cavity center and beyond. After 100 million years, long after the cavity has disappeared, the relatively dense filament extends to 20-30 kpc and the cosmic rays have diffused into a quasi-spherical lobe 40 kpc in diameter. These computed X-ray and radio features agree well with those observed in M87/Virgo and resemble those in other "relic" cluster radio sources such as Abell 13 and Abell 133. Eventually, the filament falls back and shocks at the center of the cluster – perhaps stimulating the famous non-thermal M87 jet – and only the aging radio lobe remains.

Subject headings: X-rays: galaxies – galaxies: clusters: general – X-rays: galaxies: clusters – galaxies: cooling flows

1. INTRODUCTION

The means by which accretion energy is communicated from massive black holes in cluster-centered galaxies to the surrounding hot gas are commonly thought to be fundamentally non-thermal. In galaxy clusters non-thermal energy is evidently transported and deposited in distant cluster gas via jets visible at radio frequencies. This notion is supported by numerous observations of concentrated non-thermal radio emission in young kpc-sized cavities in the hot cluster gas observed with X-rays (e.g. Bohringer et al. 1993; Fabian et al. 2000; Birzan et al. 2006; Clarke et al. 2006). A full understanding of these remarkable energy outbursts can only be achieved with quantitative observational and theoretical studies of both cosmic rays and hot thermal gas in galaxy clusters.

In Mathews & Brighenti (2007) we showed how a localized source of cosmic rays, as for example the working surface of a jet, carves out cavities in an initially uniform hot gas. When cosmic rays diffuse rapidly through the thermal gas, the cavities produced with a given total cosmic ray energy are small and tend to disappear rapidly after the cosmic ray source turns off. If the same total energy is imparted to cosmic rays that diffuse more slowly through the gas, the size of the cavities and their longevity both increase. In this case the non-thermal energy is efficiently trapped within the cavity (Churazov et al. 2001). The case of most interest probably lies between these extremes. Non-thermal radio emission from cosmic ray electrons is largely confined within cavities (or jets) at early times, but at later times the cosmic rays diffuse into the surrounding hot gas to form radio lobes with sizes much larger than the cavities.

In the exploratory calculations described here we extend our previous calculations to study the 2D evolution of cavities formed with cosmic rays in hot cluster gas confined by gravity. Because of the diffusive nature of cosmic rays and the requirement that they eventually evolve into the large radio lobes observed, the total non-thermal energy required to create typical X-ray cavities of radius r_{cav} can be much larger than the purely hydrodynamic work $\sim P4\pi r_{cav}^3/3$ required to displace uniform hot gas with pressure P.

Another, more specific motivation for the calculations described here are the *Chandra* X-ray observations of M87/Virgo by Young et al. (2002) and Forman et al. (2005; 2007) that reveal a $\sim$ 25-kpc long, nearly radial gaseous filament extending from the central galaxy M87 toward the SW. (We adopt a distance of 16 Mpc from Tonry et al. 2001.) This thermal feature, beautifully shown in Fig. 2 of Forman et al. (2007), is remarkable because it lies just along the radius of the large SW quasi-spherical "outer" radio lobe of radius $\sim$ 25 kpc observed at 90 cm with the VLA (Owen et al. 2000). This geometrical relationship between the thermal filament and radio lobe can be seen in Fig. 5 of Young et al. (2002). By including the dynamical and diffusive effects of cosmic rays, we show how X-ray cavities evolve into radial filaments surrounded by large (radio) lobes. Our calculation described here is also relevant the evolution of some "relic" radio sources observed in other clusters. According to Giovannini & Feretti (2004) these extended, steep spectrum radio sources are usually located in the outer parts of the hot cluster gas, unrelated to any non-central

[1] UCO/Lick Observatory, Dept. of Astronomy and Astrophysics, University of California, Santa Cruz, CA 95064
[2] Dipartimento di Astronomia, Università di Bologna, via Ranzani 1, Bologna 40127, Italy

galaxy. However, cosmic rays that diffuse from X-ray cavities can only produce relic radio lobes that are relatively close to the cluster core, such as those in Virgo, A13 or A133. Most relic sources are too large (400 - 1500 kpc) or too distant ($\gtrsim$ 1000 kpc) to be explained in this way.

Previous computational studies of the evolution of X-ray cavities, in which cavities filled with super-heated, non-relativistic buoyant gas are formed or placed in the hot gas cluster atmospheres, have shown that the cold gas flowing around and beneath the buoyant cavity eventually projects up through the cavity, resulting in a radially outflowing thermal feature that is cooler and more metal-rich than the surrounding gas (e.g. Reynolds et al. 2005; Gardini 2007; Ruszkowski et al. 2007; Roediger et al. 2007). We therefore envisage a cavity-lobe evolution with two jets. The first jet is an AGN jet, perhaps similar to the famous 2 kpc non-thermal jet in M87, that injects cosmic ray energy into expanding cavities. While it is commonly (even universally) assumed that X-ray cavities are formed by jets from the galactic nucleus, there is very little observational evidence of these jets. The second jet is the thermal jet that forms from the vortex flow around the buoyant cavity which, as we show here, can project to great radial distances. We shall refer to this as a "cavity jet" because of its origin and resemblance to the long radial filament visible in *Chandra* images. We show below that the cavity jet can be visible long after the associated X-ray cavity has disappeared from view and the cosmic rays that initially created it have diffused into a large (radio) lobe surrounding the cavity jet.

In our discussion of the cavity-lobe evolution that follows we have elected not to compute the radio frequency surface brightness in detail although this will be essential to fully confirm the accuracy of our proposed evolution. We impose this limitation to avoid introducing new uncertain parameters – such as the radial variation of magnetic field strength in the cluster gas, the ratio of of cosmic ray electrons to protons, synchrotron losses, etc. – that would further complicate the dynamical presentation which is sufficiently detailed already. Consequently, we shall regard our model for the radio lobe a success if the cosmic rays occupy approximately the same volume as the outer radio lobe in M87/Virgo and have enough energy to produce the radio luminosity observed. Finally, our intention is to study the physical nature of the cavity-radio lobe evolution and not attempt to solve the global cooling flow problem although the two are obviously related.

2. EQUATIONS AND COMPUTATIONAL PROCEDURE

The combined Eulerian evolution of (relativistic) cosmic rays (CRs) and thermal gas can be described with the following four equations:

$$\frac{\partial \rho}{\partial t} + \nabla \cdot \rho \mathbf{u} = 0 \tag{1}$$

$$\rho \left(\frac{\partial \mathbf{u}}{\partial t} + (\mathbf{u} \cdot \nabla)\mathbf{u} \right) = -\nabla(P + P_c) - \rho \mathbf{g} \tag{2}$$

$$\frac{\partial e}{\partial t} + \nabla \cdot \mathbf{u} e = -P(\nabla \cdot \mathbf{u}) - (\rho/m_p)^2 \Lambda \tag{3}$$

$$\frac{\partial e_c}{\partial t} + \nabla \cdot \mathbf{u} e_c = -P_c(\nabla \cdot \mathbf{u}) + \nabla \cdot (\kappa \nabla e_c) + \dot{S}_c \tag{4}$$

$$\frac{\partial \rho z_{Fe}}{\partial t} + \nabla \cdot \rho z_{Fe} \mathbf{u} = 0 \tag{5}$$

where we suppress artificial viscosity terms. Pressures and thermal energy densities in the plasma and cosmic rays are related respectively by $P = (\gamma - 1)e$ and $P_c = (\gamma_c - 1)e_c$ where we assume $\gamma = 5/3$ and $\gamma_c = 4/3$. The cosmic ray dynamics are described by e_c, the integrated energy density over the cosmic ray energy or momentum distribution, $e_c \propto \int EN(E)dE \propto \int p^4 f(p)(1+p^2)^{-1/2} dp$.

The first three equations are the usual equations for conservation of mass, momentum and energy in the hot thermal cluster gas, except we allow for optically thin radiative losses with the usual bolometric cooling coefficient $\Lambda(T, z)$ erg cm^3 s^{-1} as described by Sutherland and Dopita (1993). Note that the CR pressure gradient in equation 2 contributes to the motion of the thermal gas. This exchange of momentum between CRs and gas arises as the CRs diffuse through magnetic irregularities (Alfven waves) that are nearly frozen into the hot thermal gas. However, magnetic terms do not explicitly enter in the equations because typical magnetic fields in cluster gas $\sim 1 - 10\mu$G (Govoni & Feretti 2004) are too small, i.e. the magnetic energy densities $\sim B^2/8\pi \lesssim 10^{-11}$ erg cm^{-3} are generally much less than the thermal energy density in the hot gas. In addition, the Alfven velocity $v_A = B/(4\pi\rho)^{1/2} = 2n_e^{-1/2} B(\mu\text{G})$ km s^{-1} is typically much less than the sound or flow speeds in cluster gas so the Alfven velocity of the magnetic scatterers can be ignored (e.g. Drury & Falle 1986, Jones & Kang, 1990). Finally, the gas pressure will be isotropic, as we assume, if the scale of magnetic field irregularities is small compared to length scales of astronomical interest.

Although hot cluster gas is weakly magnetic, $\beta = 8\pi P/B^2 > 1$, the proton Larmor radius $r_L = (m_p c/eB)(2kT/m_p)^{1/2} = 4 \times 10^8 T_7^{1/2}/B_{-5}$ cm is about eleven orders of magnitude smaller than the Coulomb mean free path $\lambda = 3(3/\pi)^{1/2}(kT)^2/4n_e e^4 \ln\Lambda = 25T_7^2/n_{e-2}$ pc, where numerical subscripts refer to exponents in cgs units. Note that λ is much less than the size of most X-ray cavities. We therefore assume that the dissipationless gas dynamics equations above are appropriate for hot cluster gas and that dissipation in shocks can be treated in the normal way with artificial viscosity. The physical nature of dissipation in cluster gas is currently unclear (e.g. Lyutikov 2007).

Equation 4 above describes both the advection of CRs with the gas and their diffusion through the gas. A mass conservation equation for the CRs is unnecessary because of their negligible rest mass. The CR diffusion coefficient κ is difficult or impossible to calculate in the absence of detailed information about the magnetic field topology which is currently unknown. We expect that κ may vary inversely with the density of the thermal gas, assuming that the magnetic field strength also scales with density. For simplicity we ignore for now any dependence of κ on CR particle momentum. Since observed radio lobes are approximately spherical rather than systematically oblate or prolate, we assume that κ is isotropic, which is consistent with a highly irregular magnetic field on scales of interest here. For these preliminary calculations it is not necessary to specify the CR composition, either electrons or protons can dominate as long as they are relativistic. Finally, we assume that the total CR energy

density is not substantially reduced by losses due to synchrotron emission or interactions with ambient photons or thermal particles during the cavity evolution time. We show below that this assumption is appropriate for the Virgo cluster.

The set of equations above, including equation (5) for the conservation of iron, are solved in z, r cylindrical coordinates using a substantially modified version of ZEUS 2D (Stone & Norman 1992). The computational grid consists of 200 equally spaced zones in both coordinates out to 50 kpc plus an additional 100 zones in both coordinates that increase in size logarithmally out to ~ 2 Mpc. The initial radial variation of gas density and temperature in M87 and the surrounding Virgo galaxy cluster are taken from the analytic fits to the observations suggested by Ghizzardi et al. (2004). We choose a spherical gravitational field $\mathbf{g} = (g_z, g_r)$ that establishes exact hydrodynamic equilibrium for the corresponding (observed) gas pressure gradient. The initial abundance profile in the hot gas is that suggested by Rebusco et al. (2006). The cosmic ray diffusion term in equation 4 is solved using explicit differencing so each time step is restricted by the stability condition for the diffusion as well as the Courant condition for hydrodynamic stability.

We assume that the X-ray cavity is formed at some fixed radius by CRs supplied or produced by a non-thermal jet from the central black hole (AGN). The CRs are deposited in a gaussian-shaped sphere of characteristic radius $r_s = 2$ kpc located at $\mathbf{r}_{cav} = (0, 10\text{kpc})$, i.e. 10 kpc along the z-axis. The CR source term in equation 4 is therefore

$$\dot{S}_c = \frac{E_{ctot}}{t_{cav}} \frac{e^{-((\mathbf{r}-\mathbf{r}_{cav})/r_s)^2}}{\pi^{3/2} {r_s}^3} \quad \text{erg cm}^{-3}\text{s}^{-1} \qquad (6)$$

when $t < t_{cav}$. The integral of $(r_s \pi^{1/2})^{-3} e^{-(r/r_s)^2}$ over space is unity. In the course of these calculations we have considered several values of the total CR energy E_{ctot} and injection time t_{cav}, but we begin by describing only the flow that develops when $E_{ctot} = 1 \times 10^{59}$ ergs and $t_{cav} = 2 \times 10^7$ yrs. We also considered several other sizes for the source region, $r_s = 0.5$ and 5.0 kpc, but the computed flows and our conclusions are not sensitive to this parameter. At times $t > t_{cav}$ when $\dot{S}_c = 0$, the total CR energy $E_c = \int e_c dV$ over the grid volume remains very nearly constant at E_{ctot} but changes slightly due to advection in adiabatic compressions or rarefactions.

We have also considered a range of constant and density-dependent CR diffusion coefficients, but (unless noted otherwise) the calculations discussed below were done with the following variation with thermal electron density:

$$\kappa = \begin{cases} 10^{30} \text{ cm}^2\text{s}^{-1} & : \quad n_e \le 0.006 \text{ cm}^{-3} \\ 10^{30}(0.006/n_e) \text{ cm}^2\text{s}^{-1} & : \quad n_e > 0.006 \text{ cm}^{-3} \end{cases}$$

This $\kappa(n_e)$ is similar to the diffusion coefficients used by Mathews & Brighenti (2007) where a more complete discussion can be found. We regard κ as an adjustable parameter although our values are similar to those used in CR models of the Milky Way (e.g. Snodin et al. 2006). If the cavity jet and outer radio lobe in M87/Virgo are related, as we believe, κ must be sufficiently large so the jet and the lobe evolve on the same time scale.

3. A COSMIC RAY PLUS GAS DYNAMICAL EVOLUTION FOR M87/VIRGO

Figure 1 shows the X-ray surface brightness $\Sigma(r, z)$ and the cosmic ray energy density contours of the cavity-lobe evolution at three times. At early times (upper and central panels) $\Sigma(r, z)$ is the bolometric X-ray brightness, but at 10^8 yr the $\Sigma(r, z)$ is plotted in the soft energy 0.5 - 1 keV band where the cavity jet is illustrated in the *Chandra* images of Forman et al. (2007). The bolometric correction for this soft X-ray bandpass $BC(T) = \Lambda(T, z_{Fe}; 0.5 - 1.0 \text{ keV})/\Lambda(T, z_{Fe})$ was found using XSPEC assuming solar abundances.

The weak shock produced by the growing X-ray cavity is faintly visible in the upper and central panels of Figure 1 at 22 and 33 kpc respectively. The brightness enhancement at the shock is $\sim 20\%$, while the emission weighted temperature increases by only $\sim 5\%$. The cavity reaches its maximum size at about 2×10^7 yr when the source $\dot{S}_c$ has just turned off. A cavity of radius 5 kpc is visible in the central panel of Figure 1 centered just slightly beyond the 10 kpc CR injection radius.

Most observers estimate the energy required to form and fill a cavity of volume V as $E_{c,est} = [\gamma_c/(\gamma_c - 1)]PV = 4PV$ where P is the local pressure in the local cluster hot gas. At the CR injection radius in Virgo the gas pressure is $P = 1.3 \times 10^{-10}$ dynes and $E_{c,est} = 8 \times 10^{57}$ ergs at 2×10^7 yr when the cavity radius is 5 kpc. However, the CR energy expended at this time in our model is $E_{ctot} = 10^{59}$ ergs, about 12 times larger than $4PV$.

As the cavity forms in Figure 1, the CR pressure contours are nearly concentric with the shape of the cavity (upper and central panels). At 2×10^7 yr the cavity jet has not yet been formed, although the bottom of the cavity is clearly distorted. This flattening in the z-direction becomes more pronounced after 2×10^7 yr and by 5×10^7 yr the crosssectional shape of the buoyant cavity (now located at $z \approx 26$ kpc) resembles a banana. Meanwhile, its overall volume decreases as CRs diffuse through the cavity walls.

The cavity jet becomes clearly visible at 5×10^7 yr and grows in visibility until about 10^8 yr, seen (in the 0.5 - 1 keV bandpass) as a long bright extension along the z axis in the lower panel of Figure 1. The faint vertical feature along the r-direction at $z \approx 33$ kpc may correspond to a similar (more one-sided) feature in Fig. 2 of Forman et al. (2007). We show below that the cavity jet is visible until about 2.5×10^8 yrs. By 10^8 yr the CR energy density contours $e_c(r, z)$ are elongated along the z-axis, resembling the geometry of the large outer radio lobe in M87/Virgo.

The detailed variation of gas and CR parameters along the z (jet) axis in Figure 1 is illustrated in more detail in Figures 2 and 3. The top panel of Figure 2 at 2×10^7 yr shows the dominance of the cosmic ray pressure in the cavity region, $0.7 \lesssim \log z_{kpc} \lesssim 1.37$ ($5 \lesssim z_{kpc} \lesssim 23$ kpc). The abrupt gas pressure change at $\log z_{kpc} = 1.55$ ($z_{kpc} = 35$) is produced by the weak shock that accompanies the CR cavity formation. After 5×10^7 yr (central panel) the buoyant cavity (with radial diameter $\sim$4 kpc) is only slightly visible where $P_c \approx P$ near $\log z_{kpc} \approx 1.4$ ($z_{kpc} = 26$ kpc). Most of the CRs that supported the cavity at 2×10^7 yr have by 5×10^7 yr diffused into the

ambient gas and $P_c(r)$ has flattened considerably. At 10^8 yr the gas pressure in Figure 2 has now nearly recovered its pre-cavity profile and the cosmic ray pressure, although smaller, extends to 30-40 kpc, comparable to the size of the M87/Virgo outer radio lobe which has an estimated age of $\sim 10^8$ yr (Owen et al. 2000). Note that the initial undisturbed M87/Virgo atmosphere, shown with the same dotted profile in each panel of Figure 2, differs only very slightly from the total pressure $P_{tot} = P + P_c$ (solid lines) during most of the evolution. This confirms that the gas flow is largely subsonic.

Figure 3 shows the radial gas velocity and density profiles along the z (jet) axis at the same three times. The density $n_e(z)$ along the cavity jet departs significantly from the original (observed) profile shown with the same dotted line in all three panels. At 2×10^7 yr the density has a sharp minimum that defines the moment when the X-ray cavity has reached its maximum size, but the cavity center has moved somewhat beyond the CR injection radius (10 kpc). The weak shock is visible at 33 kpc. At 2×10^7 yr the cavity jet has not yet appeared, but at 5×10^7 yr and 10^8 yr we see a clear density enhancement in the cavity jet out to about 22 and 33-40 kpc respectively, i.e. $n_e > n_e(t = 0)$. By 5×10^7 yr the cavity at $\sim$26 kpc has filled in and become much smaller. By 10^8 yr no cavity is visible on the z axis. But at this time the dense cavity jet (dashed line) is even more pronounced compared to the original density profile (dotted line) and extends to $\sim$ 35 kpc. Higher densities in the cavity jet together with the unperturbed pressure profile in Figure 2 indicate that the cavity jet is much cooler than the surrounding gas, consistent with observations of the M87/Virgo filament (Simionescu et al. 2001; Molendi & Gastaldello 2001).

The velocity along the z axis, shown in Figure 3 with solid lines, is very strongly peaked inside the cavity at 2×10^7 yr. Although the total negative pressure gradient $d(P + P_c)/dz$ remains similar to that in the original undisturbed gas, the gas density is extremely low inside the cavity so the gas acceleration $a \approx \rho^{-1} d(P+P_c)/dz \approx \rho^{-1} dP_c/dz$ becomes enormous. High velocities are also visible in the smaller cavity at 5×10^7 yr. Since only a tiny mass is involved, these dramatic localized high velocity episodes have little influence on the overall evolution.

The radial velocity along the cavity jet at 5×10^7 yr and 10^8 yr in Figure 3 describes the dynamics and fate of this feature which is so prominent in soft X-ray images of M87/Virgo. At 5×10^7 yr the jet velocity is positive beyond 8 kpc and increases almost linearly to nearly 600 km s^{-1} at 20 kpc where the sound speed in the original atmosphere is 720 km s^{-1}. However, by 10^8 yr the jet velocity along the cavity jet is negative within about 22 kpc and is falling back toward the M87/Virgo core. The maximum velocity 200 km s^{-1} at 30 kpc is now lower. As we show below, by $\sim 3 \times 10^8$ yrs the entire cavity jet has fallen back and shocked with the dense gas at the center of M87. (It is possible that the infalling cavity jet contributed to the black hole accretion that triggered the energy outburst resulting in the younger non-thermal jet in M87.)

Figure 4 provides a snapshot of the variation of gas properties perpendicular to the cavity jet at $z = 15$ kpc and time 10^8 yr. The solid lines in these plots are profiles in the r-direction across the jet at $z = 15$ kpc. For comparison, the dashed lines are profiles in the gas (far from the jet) along the z-direction at $r = 15$ kpc. The deviation of the solid profiles from the dashed profiles shows the local variations caused by the cavity jet. In the top two panels the density and temperature (light solid lines) deviate from the undisturbed gas in opposite senses so that the pressure across the jet (third panel down) is essentially unchanged. Similar snapshot figures at other times and z distances reveal that the cavity jet is in pressure equilibrium with the surrounding gas throughout most of its evolution. The emission-weighted temperature profiles, shown with heavy lines in the second panel, confirm that the colder jet is still clearly visible when observed through the entire cluster gas.

The low entropy $S = kT/n_e^{2/3}$ and high (iron) abundance in the profiles transverse to the jet shown in Figure 4 attest that the gas in the cavity jet has come from deep within the core of M87/Virgo. As observers search for similar radial cavity jets in other clusters, they should appear as radial features of low temperature, low entropy and high abundance. These are all well-known attributes of the cavity jet in M87/Virgo.

The velocity structure transverse to the cavity jet $v_z(z = 15 \text{ kpc}, r)$ shown in Figure 4 reveals that the core of the jet at $z = 15$ kpc and time 10^8 yr is already falling back toward the M87 core while most of the gas beyond about 1.5 kpc from the jet center is still moving out. At earlier times, the jet center can also have positive velocity, but it always moves more slowly than the periphery of the jet throughout the evolution. (Note that the core velocities shown in Figure 3 may not represent the mean velocity of most of the jet gas at that radius.) The cores of the cavity jet reach their maximum radius and begin to fall back somewhat sooner than the outer (more massive) parts. This behavior is expected because at any time the cavity jet is in pressure equilibrium with the ambient gas at each radius and also shares the same gradient dP_{tot}/dz along the jet. Consequently, the outward acceleration of gas in the jet $a \approx \rho^{-1} dP_{tot}/dz$ is therefore always less in the core of the jet where the density is greatest.

Figure 5 shows X-ray surface brightness profiles $\Sigma(z, r)$ in the soft 0.5 - 1.0 keV band similar to that illustrated in Fig. 4 of Forman et al. (2007) for the M87/Virgo filament. The solid lines show $\Sigma(r)$ at fixed values of z that label the curves; these illustrate the decrease in X-ray surface brightness proceeding from the center of the cavity jet in a perpendicular direction. For comparison, the dashed lines show $\Sigma(z)$ far from the jet at the same radius r labeled in each panel. As time progresses the half-width of the computed filament in Figure 5 slowly shrinks until, at 3×10^8 years the entire filament (and most of its iron) has fallen back to the core of M87. The observed surface brightness enhancement in M87/Virgo at 10 kpc along the jet is (shown in Fig. 4 of Forman et al.) has a maximum contrast to the local gas of about 20 - 30 percent (or 0.08 - 0.12 in $\log \Sigma$) and the half-width is 5-10″ (0.4 - 0.8 kpc). Our calculated cavity jet (filament) has similar properties but is somewhat broader and more luminous than that in M87/Virgo. The occasional multiplicity of peaks in Figure 5 also appears in the M87/Virgo observations, but such irregularities would be expected in the more active environment of a

real cluster. As a check, we repeated the cavity jet calculation at higher resolution using a numerical grid about three times smaller and the features shown in Figures 4 and 5 were essentially unchanged.

Cooling by radiation losses in equation 3 does not strongly influence our results. In some of our cavity jet calculations we found that at time 10^8 yrs the radiative cooling time in the cavity jet $t_{cool} = 5m_pkT/2\mu\rho\Lambda$ was also $\sim 10^8$ yrs. However, as the calculation proceeded, adiabatic cooling continued to dominate and the radiative cooling time t_{cool} eventually increased faster than the time elapsed. Although t_{cool} in the cavity jet can pass through a minimum, no gas cooled to very low temperatures. It is possible that radiative cooling to low temperatures may occur with somewhat different cluster and cavity parameters. In addition, after a few 10^8 yrs a small mass of gas cooled near the origin, but this has no effect on the results discussed here.

Figure 6 illustrates rather dramatically the (temporary) transport of low entropy, metal-rich gas in the cavity jet from the central core to large distances in the hot cluster gas at 10^8 yr. The entropy and abundance along the filament core are both remarkably constant out to 30-40 kpc, showing little effects due to numerical diffusion. This near constancy of the entropy is possible only if the filament gas expands adiabatically without experiencing shocks.

4. RADIO SYNCHROTRON EMISSION IN M87/VIRGO OBSERVED AND ESTIMATED

We now inquire if the cosmic ray energy density $e_c(r, z)$ shown at 10^8 yr in Figures 1 and 2 is sufficient to emit the radio luminosity observed in the M87/Virgo halo. The half life for relativistic electrons to synchrotron losses is $t_{1/2} \approx 25/B^2\gamma_L$ yrs, where for simplicity the Lorentz factor γ_L is assumed to be the same for all electrons. Taking the mean field in M87/Virgo to be $B = 10\mu$G (e.g. Owen et al. 2000) and imposing $t_{1/2} = 10^8$ yrs, we find $\gamma_L \approx 2500$. The total synchrotron power from each electron is $P_{syn} = (4/3)\gamma_L^2 c\sigma_T(B^2/8\pi) = 7 \times 10^{-19}$ erg s^{-1}. The mean number density of relativistic electrons n_c can be estimated using $n_c\gamma_L m_e c^2 = e_c = 3P_c \approx 3 \times 10^{-11}$ erg cm^{-3}, taken from the $t = 10^8$ year panel in Figure 2. It follows that $n_c \approx 1.5 \times 10^{-8}$ cm^{-3} so the total emissivity from all electrons is $n_cP_{syn} \approx 10^{-26}$ erg cm^{-3} s^{-1}. Then we estimate the total radio luminosity from the radio lobe (of radius $r_{lobe} \approx 35$ kpc) to be $L \approx n_cP_{syn}(4/3)\pi r_{lobe}^3 \approx 5 \times 10^{43}$ erg s^{-1}.

The total radio luminosity observed in M87/Virgo from 10MHz to 150GHz is 9×10^{41} ergs s^{-1} (Herbig & Readhead 1992). However, we estimate the luminosity of the radio halo alone, 1.5×10^{41} erg s^{-1}, by integrating the halo flux densities tabulated by Andernach et al. (1979) from 0.1 to 10GHz.

We see that the observed radio luminosity is about 300 times less than our rough idealized estimate. This suggests that a more detailed radio synchrotron model consisting of a range of relativistic electron energies and including relativistic protons can be designed to fit the radio data. We do not attempt such a detailed model at present since it introduces additional sensitive, poorly known parameters, such as the radial dependence of the magnetic field.

One possible concern with our treatment of CR diffusion is that the dimensions of the large radio halo in M87/Virgo would be similar at all radio frequencies. If more energetic electrons diffuse appreciably faster, as might be expected, the size of the radio halo could vary with frequency (Owen et al. 2000). However, the energy estimates above suggest that a wide energy spectrum of secondary electrons can be produced throughout the outer lobe by pion production from cosmic ray protons. Owen et al. (2000) also note that the outer boundary of the radio halo appears sharper than might be predicted by a standard diffusion model. However, the physical nature of the CR diffusion coefficient is still largely unknown and is likely to differ from the vanilla diffusion considered here. To better understand cosmic ray diffusion, we urge radio observers to determine the precise shape of the "sharp" outer boundary of the outer lobes in M87/Virgo at several radio frequencies.

The shape and size of the cosmic ray lobe depends sensitively on the diffusion coefficient $\kappa(n_e)$. We illustrate one example of this in Figure 7 which shows athe CR contours (and soft X-ray image) at time 10^8 yr in a calculation similar to that shown in Figure 1 but different in two respects: (1) the total CR energy is reduced to $E_{ctot} = 5 \times 10^{58}$ ergs to keep the cavity size at 2×10^7 yrs similar to that in Figure 1, and (2) the CR diffusion coefficient is lowered as follows:

$$\kappa = \begin{cases} 10^{29} \text{ cm}^2\text{s}^{-1} & : \quad n_e \le 0.008 \text{ cm}^{-3} \\ 10^{29}(0.008/n_e)^{1.14} \text{ cm}^2\text{s}^{-1} & : \quad n_e > 0.008 \text{ cm}^{-3} \end{cases}$$

With this lower $\kappa(n_e)$, the CR contours (if symmetric about the $z = 0$ plane) more clearly define two separate cosmic ray (outer radio) lobes that have sharper edges. The thermal cavity jet is comparable in brightness and other properties to the one we have described in detail above.

5. CAVITY JETS AND "RELIC" RADIO SOURCES IN OTHER CLUSTERS

Many galaxy clusters contain extended, steep spectrum "relic" radio source located far from the cluster-centered galaxy but which are unassociated with any line of sight galaxy near the source (Giovannini & Feretti 2004). The dimensions and locations of relic sources vary considerably, but most relics are extremely large ($\gtrsim$ 500 kpc) and very distant ($\sim$ 1000 kpc) from the cluster center. One much-discussed origin for giant relic sources are merger-related shocks that re-energize latent cosmic ray electrons in the cluster gas (e.g. Pfrommer, Ensslin, Springel, 2007). However, there is a subclass of smaller relics – like those in A13, A85, A133, A4038 (Feretti & Giovannini 2007) – that often lie within or near X-ray detectable cluster gas, and are therefore relevant to our calculations here. To our knowledge the outer radio lobes of M87/Virgo have not been classified as relic sources, but they resemble relics in many ways except we view them projected against the cluster-centered galaxy M87. The outer lobes in M87/Virgo may be younger than most relics. If the magnetic field decreases with cluster radius (and CR electron lifetimes increase), radio electrons closer to the cluster center will be lost and the mean radius of the M87/Virgo lobes will increase with time.

The cluster A133 contains a relic radio source (Slee et al. 2001) located about 40 kpc NW of the cluster center and *Chandra* observations show an extended filament

of relatively cool gas proceeding radially from the cluster core to the relic source (Fujita et al. 2002). This is the same radio and X-ray configuration we show in Figures 1 (bottom panel) and 7. The mean gas temperature in A133 rises from 2 keV at a few kpc to 4.5 keV at 110 kpc, but the temperature of the dense thermal filament is lower (e.g. less than 2 keV at ~ 20 kpc). X-ray and radio observations of A13, another similar but perhaps more complicated cluster, have been discussed by Juett et al. (2007). In A13 a broad radial filament of cooler gas connects the cluster core to the relic radio source at ~ 300 kpc. The authors of these papers suggest that while the radio emission probably comes from a central AGN, the cool filaments either result from a recent merger or from an "uplifting" of cooler gas from the cluster core. We prefer to think that radio relics and radial X-ray filaments are both natural outcomes of cavities formed by cosmic rays.

6. CONCLUDING REMARKS

Radial jet-like thermal filaments and associated large radio lobes evolve from X-ray cavities that are inflated with cosmic rays that eventually diffuse through the cavity walls. The radio features created from cavity CRs are unlike either FRI or FRII morphologies, where non-thermal energy flows directly from the central black hole. In general cavities and cavity jets are not likely to coexist. X-ray cavities containing cosmic rays that later diffuse into larger radio lobes are likely to be observed early-on as they are being filled with cosmic rays or shortly thereafter. By the time the cosmic rays have diffused from an X-ray cavity to fill a large radio-emitting volume in the cluster gas, the initial cavity will have disappeared. The radio lobes will be accompanied for $\gtrsim 2\times10^8$ yrs by nearly radial, low temperature, low entropy, metal rich thermal filaments similar to the M87/Virgo filament seen in *Chandra* images.

Since X-ray cavities are observed in about 20 percent of all clusters (Birzan et al. 2004), it may be surprising that the fraction of clusters like M87/Virgo, A13 and A133 with cavity jets is much smaller. Moreover, the double outer radio lobes in M87/Virgo appear to be nearly identical radio sources symmetric about the center of M87, but only one lobe has a cavity jet. If the filaments last about 4-5 times longer than X-ray cavities, as in our model, the number of cluster filaments should be larger by the same factor, but this has not been observed to date.

The initial position of the cavity does not seem to have a large effect on the development or X-ray visibility of cooler cavity jets over times $\sim 10^8$ yrs. To explore this we repeated the calculation described in Figure 7 but with the initial cavity formed at $z = 20$ kpc instead of 10 kpc. In this case the cavity jet was broader and remained visible for slightly longer times (but with a somewhat lower amplitude). The cavity jet is visible from well within 20 kpc from the center of M87/Virgo to 30 kpc and beyond. The CR energy density $e_c(r, z)$ at time 10^8 yrs resembles that in Figure 7 but with contours shifted out by ~ 10 kpc along the z-axis.

Evidently many cluster filaments have been missed because most X-ray clusters are much fainter than M87/Virgo and have not been observed with deep, $\sim$1000 ksec *Chandra* exposures. If the CR diffusion coefficient κ is larger than our values for M87/Virgo, the cavities will be smaller for given E_{ctot} and their lifetimes may be too short to form cavity jets. Nevertheless, we hope that our calculations will inspire a more dedicated search for additional cavity jets in X-ray cooling core clusters having large diffuse radio lobes. Combined observations of thermal filaments and diffuse radio lobes can be used to date the explosive events from which they both evolved and to study in detail the propagation of cosmic rays, the magnetic structure in the hot gas and the total cosmic ray energy involved. If M87/Virgo is typical, the total energy of cosmic rays released E_{ctot} can exceed the work necessary to simply form and fill the cavities, $E_{c,est} = 4PV$, by more than an order of magnitude.

The hot gas in the Virgo cluster is currently experiencing a sequence of strong – and very different – energy releases from the central black hole. In addition to the cavity jet event discussed here, the more famous (and more recent) 2 kpc jet is moving in a NW direction unrelated to the orientation of the cavity jet and its large radio lobes. In addition, a strongly buoyant mushroom-shaped flow directly to the East of M87 is seen in both X-rays and radio images (Churazov et al. 2001). Ruszkowski et al. (2007) propose that an intensified magnetic field in the buoyant stem of this flow has caused it to be prominent in the 90 cm radio image of Owen et al. (2000). However, the cavity jet in the *Chandra* image of M87/Virgo does not appear in this radio image. This difference in the magnetic field strength may result because the gas in the Eastern plume originated deeper within the cluster gas than that in the cavity jet, assuming that the field strength increases (with gas density) toward the cluster core.

In addition to these three energy outflows associated with strong radio emission, a number of less energetic outflows from the core of M87 are apparent in optical emission. Fig. 2 of Young et al. (2002) shows the central 7 × 7 kpc region of M87/Virgo at three very different frequencies: *Chandra* X-ray, 6 cm radio and optical emission in the Hα + [NII] lines. The optical line emission is particularly interesting because about 5 plumes of warm ($T \sim 10^4$ K) gas can be seen emanating from the M87 core, all in different directions. The brightest of these is a Hα + [NII] feature that lies just North of the bright 2 kpc non-thermal jet, but at a slightly different angle. We see a parallel here with the dusty plume we have discovered and discussed in the X-ray bright galaxy group NGC 5044 (Temi, Brighenti & Mathews 2007). The NGC 5044 feature can be understood as dusty buoyant gas heated near the central black hole that is rapidly cooled to $\sim 10^4$ K by electron-dust cooling. It seems entirely plausible that the warm gas Hα + [NII] features in M87 are created in the same manner, adding to the already wide diversity of energy releases in this remarkable galaxy/cluster.

We expect that the numerous intermittent energy events seen in M87/Virgo have created subsonic velocities throughout the hot gaseous atmosphere. By contrast, our cavity jet was computed starting with stationary cluster gas exactly in hydrodynamic equilibrium and this results in a perfectly axisymmetric flow that may differ in detail from that observed in M87/Virgo. For example, the slight curvature of the cavity jet visible in Fig. 2 of Forman et al. (2007) could arise from either

from a small velocity perpendicular to the accelerating jet or from an initial velocity asymmetry near the base of the pre-filament cavity that slightly altered the direction of the cavity jet as it formed. Similarly, the "braided" nature of this filament seen in the *Chandra* image (Fig. 3 in Forman et al. 2007) may result from small random transverse velocities present when the X-ray cavity was formed.

Studies of the evolution of hot gas in elliptical galaxies at UC Santa Cruz are supported by NASA grants NAG 5-8409 & ATP02-0122-0079 and NSF grant AST-0098351 for which we are very grateful.

REFERENCES

Andernach, H., Baker, J. R., von Kap-herr, A. & Wielebinski, R. 1979, A&A, 74, 93

Birzan, L., McNamara, B. R., Carilli, L., Nulsen, P. E. J. & Wise, M. W. 2006, (arXiv:astro-ph/0612393)

Birzan, L., Rafferty, D. A., McNamara, B. R., et al. 2004, ApJ, 607, 800

Bohringer, H., Voges, W., Fabian, A. C. et al. 1993, MNRAS, 264, L25

Churazov, E., Bruggen, M., Kaiser, C. R., et al. 2001, ApJ, 554, 261

Clarke, T., Blanton, E., Sarazin, C., et al. 2006 (arXiv:astro-ph/0612595)

Drury, L. O. & Falle, S. A. E. G., 1986, MNRAS, 223, 353

Fabian, A. C., Sanders, J. S., Ettori, S. 2000, MNRAS, 318, L65

Feretti, L. & Giovannini, G. 2007, to be published in Springer Lecture Notes in Physics, "Panchromatic View of Clusters of Galaxies and the Large-Scale Structure", Editors M. Plionis, O. Lopez-Cruz, and D. Hughes (arXiv:astro-ph/0703494)

Forman, W., Jones, C., Churazov, E. et al. 2007, ApJ, 665, 1057

Forman, W., Nulsen, P., Heinz, S., et al. 2005, ApJ, 635, 894

Fujita, Y., Sarazin, C. L., Kempner, J. C., et al. 2002, ApJ, 575, 764

Gardini, A. 2007, A&A, 464, 143

Giovannini, G. & Feretti, L. 2004, Korean Astron. Soc., 37, 323

Govoni, F. & Feretti, L. 2004, Intenational Journal of Modern Physics D, 13, 1549

Ghizzardi, S., Molendi, S., Pizzolato, F. & De Grandi, S. 2004, ApJ, 609, 638

Herbig, T. & Readhead, A. C. S. 1992, ApJS, 81, 83

Jones, T. W. & Kang, W. 1990, ApJ, 363, 499

Juett, A. M., Sarazin, C. L., Clarke, T. E., et al. 2007, ApJ (in press) (astro-ph/arXiv:0708.2277)

Lyutikov, M. 2007, ApJ, (submitted) (arXiv:0709.1712)

Mathews, W. G. & Brighenti, F. 2007, ApJ, 660, 1137

Molendi, S. 2002, ApJ, 580, 815

Molendi, S., & Gastaldello, F. 2001, A&A, 375, L14

Owen, F. N., Eilek, J. A., & Kassim, N. E. 2000, ApJ, 543, 611

Pfrommer, C., Ensslin, T. A., & Springel, V. 2007, MNRAS (submitted) (arXiv:astro-ph/0707.1707)

Rebusco, P., Churazov, E., Bohringer, H. & Forman, W. 2006, MNRAS, 372, 1840

Reynolds, C. S., McKernan, B., Fabian, A. C. et al. 2005, MNRAS 357, 242

Roediger, E., Brüggen, M., Rebusco, P., Böhringer, H. & Churazov, E. 2007,MNRAS, 375, 15

Ruszkowski, M., Ensslin, T. A., Bruggen, M. et al. 2007, MNRAS, 378, 662

Simionescu, A., Bohringer, H., Bruggen, M., & Finoguenov, A., 201, A&A, 465, 749

Slee, O. B., Roy, A. L., Murgia, M. et al. 2001, AJ, 122, 1172

Snodin, A. P., Brandenburg, A., Mee, A. J. & Shukurov, A. 2006, MNRAS, 373, 643

Stone, J. M. & Norman, M. L. 1992, ApJS, 80, 753

Sutherland, R. S. & Dopita, M. A. 1993, ApJS, 88, 25

Temi, P., Brighenti, F., & Mathews, W. G. 2007, ApJ, 666, 222

Tonry, J. et al. 2001, ApJ, 546, 681

Young, A. J., Wilson, A. S. & Mundell, C. G. 2002, ApJ, 579. 560

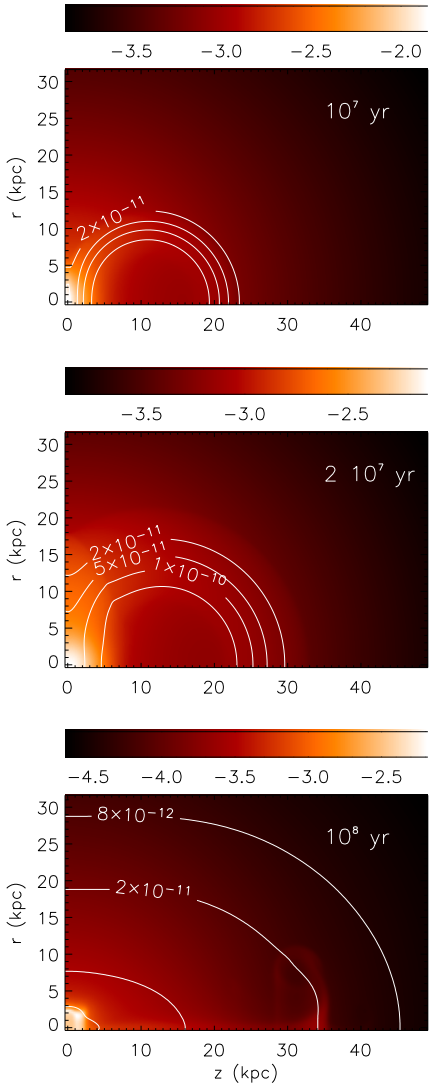


FIG. 1.— X-ray surface brightness images from computed models at three times: 10^7, 2×10^7 and 10^8 yrs. The cavity and jet are formed on the horizontal (z) axis. For the first two times the bolometic surface brightness $\Sigma(r, z)$ (in ergs cm^{-2} s^{-1}) is shown and calibrated in the color bars (upper two panels). At 10^8 years (lower panel) the surface brightness is restricted to the 0.5 - 1 keV bandpass to reveal the colder jet filament along the z axis. Each plot shows the following contours of the cosmic ray energy density $e_c(r, z)$ (from the inside out): at 10^7 yrs: 2×10^{-11}, 5×10^{-11}, 10^{-10}, and 2×10^{-10}; at 2×10^7 yrs: 2×10^{-11}, 5×10^{-11}, 10^{-10}, and 2×10^{-10}; at 10^8 yrs: 8×10^{-12}, 2×10^{-11}, 5×10^{-11}, and 8×10^{-11}, all in ergs cm^{-3}.

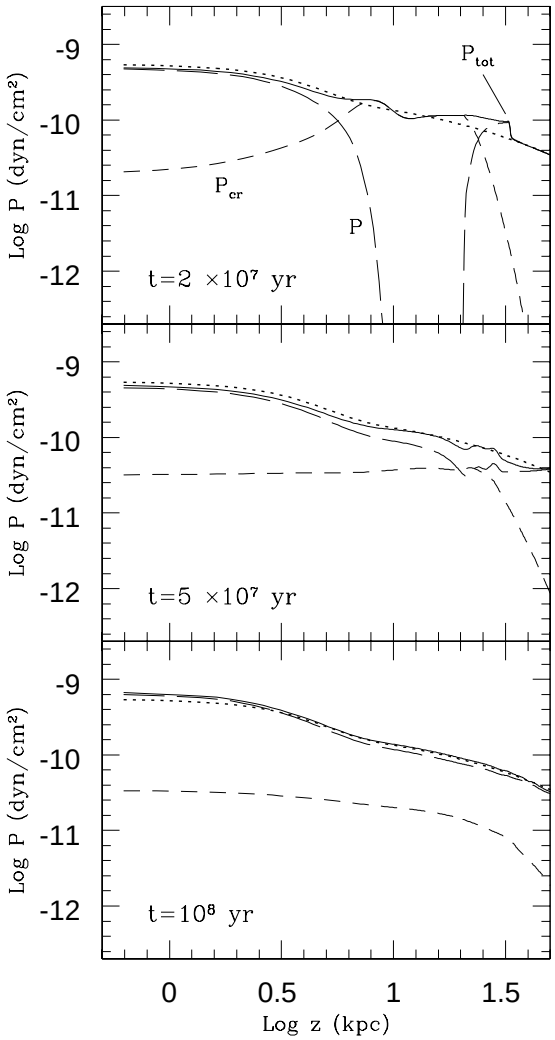


FIG. 2.— Variation of pressures along the center of the cavity jet (z axis) at three times: 2×10^7 yrs (top panel), 5×10^7 yrs (middle panel), and 10^8 yrs (bottom panel). Each panel shows the gas pressure P (long dashed lines), cosmic ray pressure P_c (short dashed lines), total pressure $P + P_c$ (solid lines). Also shown is the gas pressure profile in the initial undisturbed M87/Virgo atmosphere before the cavity was created (dotted lines).

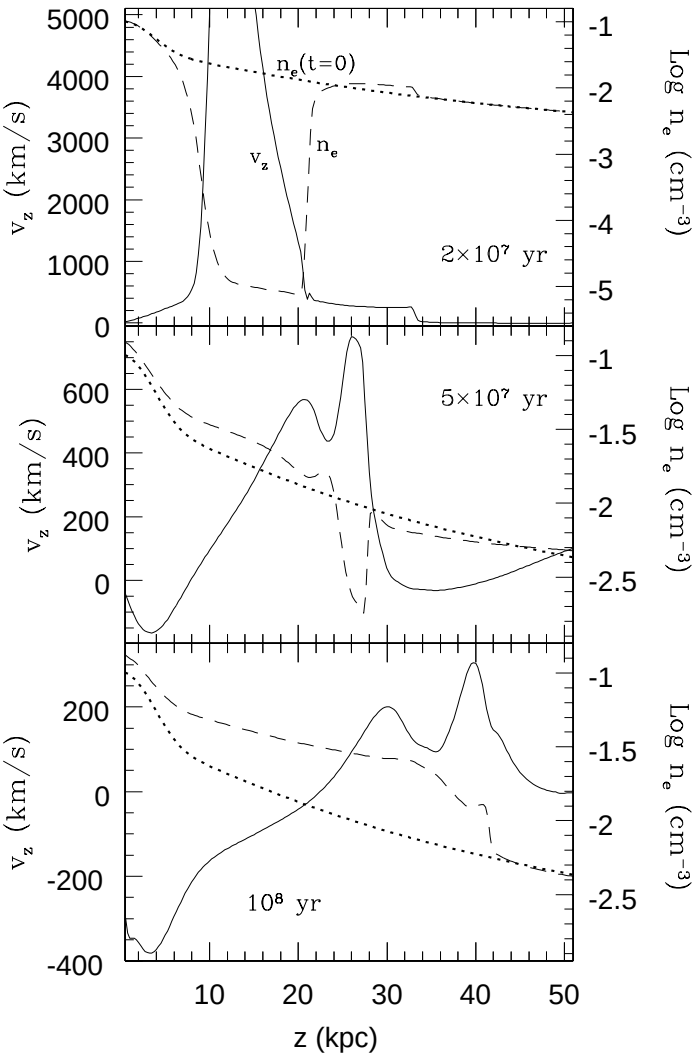


FIG. 3.— Variation of electron density n_e (dashed lines) and gas velocity v_z (solid lines) along the center of the cavity jet (z axis) at three times. Also shown is the electron density n_e profile in the initial undisturbed M87/Virgo atmosphere (dotted lines).

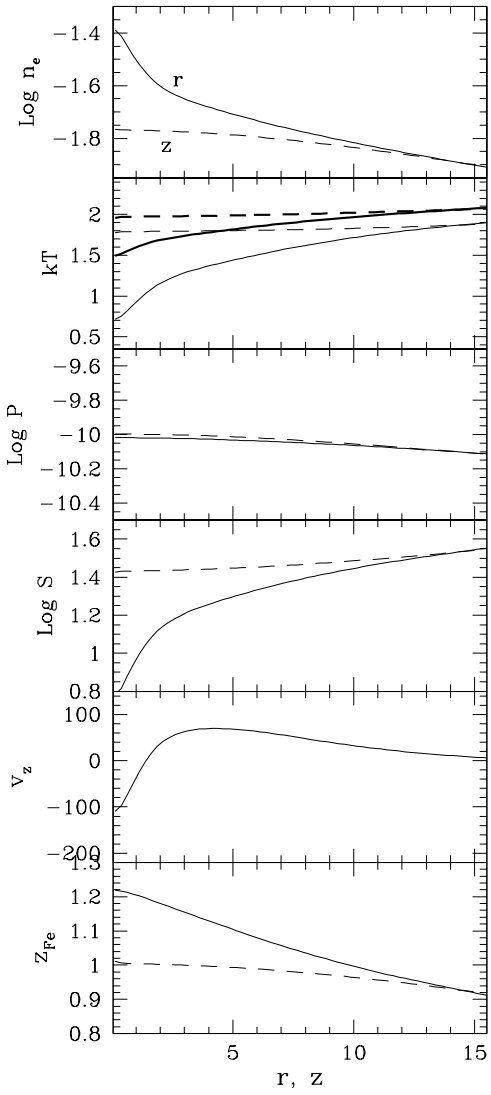


FIG. 4.— Light solid lines show profiles in the r-direction of the electron density n_e (cm^{-3}), kT (keV), gas pressure P (dynes), entropy $S = kT/n_e^{2/3}$ (keV cm^{-2}), velocity v_z (km s^{-1}), and iron abundance z_{Fe} (solar units) perpendicular to the cavity jet at $z = 15$ kpc at time 10^8 yrs. For comparison the dashed lines show the profiles in the z-direction at $r = 15$ kpc at the same time far from the jet. The heavy solid and dashed lines show the variation of the emission-weighted temperature when viewed through the entire M87/Virgo atmosphere.

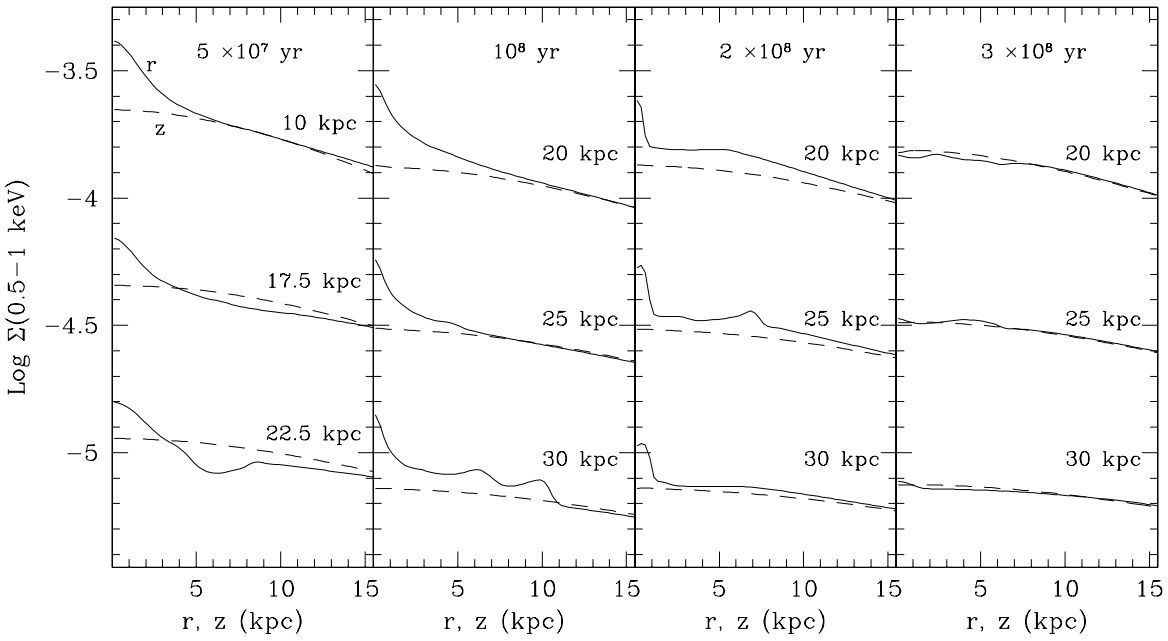


FIG. 5.— Profiles at four times of the soft X-ray surface brightness of M87/Virgo $\Sigma(r, z)$ (0.5 - 1 keV) perpendicular to the cavity jet along the z axis compared with $\Sigma(r, z)$ along the r axis far from the jet. Solid lines show the variation of Σ (erg cm^{-2} s^{-1}) in the r-direction perpendicular to the jet at distances z along the jet that label each curve. Dashed lines show the variation of Σ in the z-direction perpendicular to M87/Virgo (far from the jet) at distances r along the r-axis that label each curve. For visibility each of the three profile pairs in the panels has been arbitrarily shifted vertically so the scale is only relative.

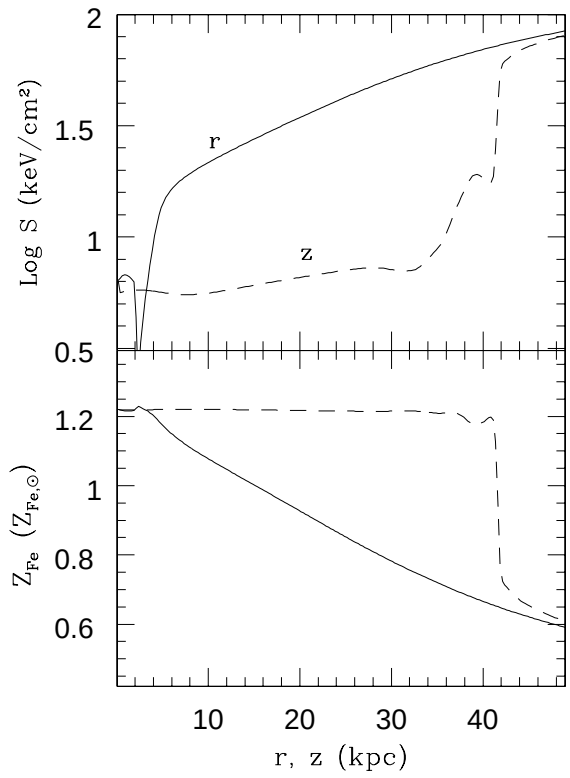


FIG. 6.— Radial profiles at time 10^8 yrs of the entropy $S = kT/n_e^{2/3}$ (keV cm^{-2}) and iron abundance z_{Fe} (solar units) directly along the jet (z-axis) shown with dashed lines and far from the jet (r-axis) shown with solid lines.

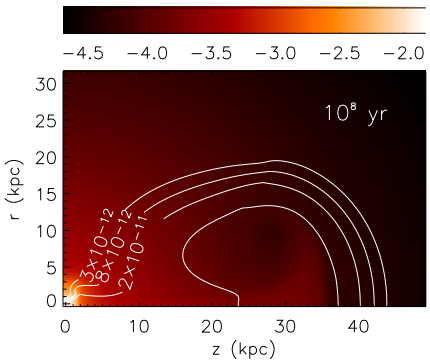


FIG. 7.— X-ray surface brightness $\Sigma(r,z)$ (erg cm^{-2} s^{-1}) in the 0.5 - 1 keV bandpass at time 10^8 yrs for a calculation identical to that shown in the lower panel of Figure 1 except a with somewhat lower cosmic ray diffusion coefficient (see §4) and a lower $E_{ctot} = 5 \times 10^{58}$ ergs. The cosmic ray energy density $e_c(r,z)$ is shown with contours (from the outside in) at 3×10^{-12}, 8×10^{-12}, 2×10^{-11}, and 6×10^{-11}, all in ergs cm^{-3}.